SUPPORTING INFORMATION

Additional Details of Methods

Bacterial Strains, Growth Conditions, and Materials

Four *E. coli* strains were used (Table 1). The background strain of *E. coli* (wild type, denoted strain "WT") is MG1655 in all cases. The doubling time of MG1655 in EZRDM at 30°C was 50 min. For experiments on cells that export GFP to the periplasm (strain "WT-ppGFP"), TorA-GFP was expressed from the plasmid pJW1 as previously described.[1] The plasmid carries the gene for GFP with the twin-arginine-translocase (TAT) signal peptide appended to its N-terminus. TAT recognizes the signal peptide and exports the properly folded GFP to the periplasm, where it can freely diffuse. This strain had a doubling time of 51 min. To construct a deletion mutant strain lacking the osmoprotectant importer ProP (strain "Δ*proP*"), we obtained strain JW4072 from the KEIO collection.[2] We transduced the kanamycin resistance gene in JW4072 that is in place of *pro*P into our background strain MG1655 via P1 transduction. The doubling time of this strain was 50 min. To visualize the permeabilization of membranes in Δ*proP*, we transformed pJW1 into Δ*proP* and expressed periplasmic GFP using the same protocol (strain "Δ*proP*-ppGFP"). The doubling time of Δ*proP*-ppGFP was again 50 min.

Bulk cultures were grown in EZ rich, defined medium (EZRDM),[3] which contains a MOPS-buffered solution supplemented with metal ions (M2130; Teknova), glucose (2 mg/mL), amino acids and vitamins (M2104; Teknova), nitrogenous bases (M2103; Teknova), 1.32 mM K_2HPO_4, and 76 mM NaCl. Cultures were grown from glycerol frozen stock to stationary phase overnight at 30°C. Subcultures were grown to exponential phase (OD = 0.2–0.6 at 600 nm) before sampling for the microscopy experiments at 30°C, unless otherwise specified.

Minimum Inhibitory Concentration (MIC) assay

The MIC for **MM$_{63}$:CHx$_{37}$** against the strains WT and Δ*proP* was determined using a broth microdilution method as previously described.[4] Results are shown in Fig. S1. Two-fold serial dilutions of **MM$_{63}$:CHx$_{37}$** in EZRDM were performed in separate rows of a polystyrene 96-well plate with each well containing an inoculum of the *E. coli* strain. The inoculum was a 1:20 dilution from a stationary culture grown at 30°C. The plate was incubated at 30°C for 6 hr for aerobic MIC measurements. The MIC values were taken as the lowest concentration for which no growth was discernible (<0.05 OD) after 6 hr. The aerobic MIC value against WT cells was 25 μg/mL. The molecular weight of an "average" copolymer (35 subunits long, 37% **CHx**, 63% **MM** sidechains) would be ~6.8 kDa. Thus an MIC of 25 μg/mL corresponds to a molar concentration of about 4 μM. Under anaerobic conditions,[5] the MIC value for the WT strain was >200 μg/mL, at least 8 times higher than in aerobic conditions. We repeated the same MIC assay on the Δ*proP* strain under aerobic conditions and obtained the value 6.25 μg/mL, which is four-fold smaller than the aerobic MIC for the WT strain.

Microfluidics Chamber for Time-Lapse Measurement

Imaging of individual cells was carried out at 30°C in a simple microfluidics chamber consisting of a single rectilinear channel of uniform 50 μm height and 6 mm width, with a channel length of 11 mm.[5] The total chamber volume is 10 μL. The negative of the cell design was patterned onto a silicon wafer via photolithography and the wafer was silanized. Sylgard 184 silicone elastomer mixture (Dow Corning) was poured onto the patterned silicon wafer and baked for 30 min in a 110°C oven after removing air in a vacuum desiccator. The cured polydimethylsiloxane (PDMS) slab was removed and holes were punched for entry and exit

hypodermic needles. The patterned PDMS slab was fused to a dried, acetone-cleaned, 22-mm × 40-mm glass coverslip pre-cleaned by plasma oxidation. Soon after the bonding of the two pieces, 0.01% poly-*L*-lysine (molecular weight >150,000 Da) was injected into the chamber for 30 min and then rinsed thoroughly with Millipore water. For imaging experiments, the chamber was maintained at 30°C with a TC-344B dual automatic temperature controller through the CC-28 cable assembly attached to RH-2 heater blocks (Warner Instruments).

Microscopy

Single-cell imaging was performed on a Nikon Eclipse Ti inverted microscope with a 100X, 1.45 N.A. phase contrast objective (Nikon), using epi illumination. An optically pumped semiconductor laser (Coherent) at 488 nm was expanded to illuminate the field of view uniformly. The laser intensity at the sample was ~5 W/cm^2. Fluorescence images were obtained with an EMCCD camera, either Andor iXon 897 or Andor iXon 887. The pixel size corresponds to 160 ± 10 nm at the sample. GFP fluorescence was imaged using the emission filter ET525/50M (Chroma).

The sequence of membrane permeabilization events caused by the copolymer can be monitored by changes in the intensity and spatial distribution of periplasmic GFP over time.[5-7] For the microscopy experiments on WT-ppGFP cells, we used 30 μg/mL of **MM_{63}:CHx_{37}** (1.2X WT MIC). A value slightly larger than the MIC was used to account for possible errors in the MIC assay. WT-ppGFP cells were injected into the microfluidics chamber. The base of the chamber was coated with poly-L-lysine to immobilize the cells. The immobilized cells were then observed in continuously refreshed, aerated medium for 5 min to ensure that the cells are growing properly prior to the injection of **MM_{63}:CHx_{37}**. On excitation at 488 nm, the resulting

image of the cells exhibits a halo of green fluorescence, indicating a predominantly periplasmic spatial distribution of GFP (Fig. 2A).

The fluorescence images are interleaved with phase contrast images every 6 s (total imaging cycle time of 12 s). The phase contrast images are used to measure cell length vs time to a precision of ±50 nm. Cell length is affected both by genuine growth and by osmotic effects, as described in the main text. The method of cell length measurement was described previously.[5]

To test for oxidative stress, we added copolymer plus the permeable, oxidation-sensitive dye CellROX Green.[5] Reduced CellROX (as added) is a membrane permeable profluorophore with weak fluorescence. *In vitro*, oxidation of CellROX by the powerful oxidants superoxide (O_2^-) or hydroxyl radical (•OH) in the presence of ds-DNA induces strong CellROX fluorescence (excited at 488 nm and detected at 525 ± 25 nm). The weaker oxidant H_2O_2 does not induce CellROX fluorescence. The affinity of CellROX for DNA prevents the dye from escaping after permeabilization of the bacterial membranes, enabling us to detect oxidative damage inside of single cells. Additional details are provided in our recent study of CM15.[5]

Cytoplasmic Membrane Permeabilization Localized to One Pole

In previous studies with the natural AMPs LL-37[6] and Cecropin A,[7] we observed localized CM permeabilization near the endcaps or the septation plane of *E. coli*. We tested whether WT-ppGFP cells under copolymer treatment also exhibit localized CM permeabilization. To enable easy visualization of the diffusive motion of periplasmic GFP at a 10 Hz frame rate, we pre-treated the cells with 60 μg/mL of cephalexin for 30 min. Cephalexin prevents septation, causing the cells to filament without hampering their overall growth. The increased cell length allows accurate monitoring of the changes in GFP spatial distribution after the copolymer treatment.

We initiated flow of the copolymer at 30 μg/mL (1.2X WT-MIC) and observed changes in the GFP spatial distribution, imaging at 10 Hz (0.1 s per camera frame, see Movie S4). As for cells that have not been pre-treated with cephalexin, in pre-treated cells GFP first accumulates at both poles (periplasmic bubbles). After a lag time of several minutes, GFP abruptly begins to enter the cytoplasm *at one endcap* (Fig. 3). This behavior is clearly shown by the GFP axial intensity profile vs time. For the typical cell shown, essentially complete drainage of GFP from the endcap near the permeabilization site occurred in ~2 s. Drainage of GFP from the second endcap, distal to the permeabilization site, occurred much more slowly, over ~60 s. Evidently the second endcap drains by diffusion of the GFP along the thin, annular length of the periplasm to the first endcap, the site of permeabilization of the CM. The data thus strongly suggest that the CM permeabilization by the copolymer is localized at one pole. Intriguingly, our observations also indicate that once permeabilization has occurred near one CM endcap, the other endcap remains impermeable. No second localized permeabilization step is observed during the period of complete redistribution of the GFP signal into the cytoplasm.

Active Respiration Required for Partial Length Recovery

At 30 μg/mL of **MM_{63}:CHx_{37}** (1.2X WT MIC), during Phase 2 the cells lengthen for a variable amount of time until CM permeabilization occurs. If this partial recovery of cell length is related to active osmoregulation, we reasoned that it should depend on respiration, which maintains the proton-motive force (pmf) and enables biosynthesis of ATP. This in turn allows the cell to import ions (K^+ and Glu^-) and osmoprotectants (Pro and glycine betaine, if present in the medium) into the cytoplasm against the chemical gradient.[8-11]

To test this hypothesis, we pre-treated WT-ppGFP cells with both carbonyl cyanide *m*-chlorophenyl hydrazone (CCCP) at 200 μM and α-deoxyglucose at 1 mM for 10 min prior to

the onset of the flow of copolymer. CCCP dissipates the pmf by transporting protons from the periplasm to the cytoplasm.[12] Deoxyglucose is imported and blocks normal glycolysis, preventing production of ATP by glycolysis.[13] After pre-treatment but prior to injection of 30 μg/mL of **MM_{63}:CHx_{37}**, we observed no growth of the cells, consistent with the halting of active respiration. Then we flowed the copolymer solution over the pretreated cells. Much like the respiring cells (Fig. 4A), the non-respiring cells shrank in length by ~10% and formed periplasmic bubbles (Fig. 4B). Evidently the initial shrinkage (Phase 1) does not require ATP or the pmf, although the shrinkage occurred more slowly in general. Unlike the respiring cells, for the non-respiring cells we observed no recovery of the cell length after the shrinkage; Phase 2 was absent.

For the non-respiring cells, CM permeabilization occurred after a variable time lag for >85% of the cells, indicating that active respiration is not required for the CM permeabilization step. In addition, for the non-respiring cells the total GFP fluorescence intensity remained constant even after GFP had entered the cytoplasm (Fig. 4B)—no abrupt decrease was observed. This observation supports our hypothesis that the sudden ~15% decrease in GFP intensity observed in *respiring* cells (which are maintaining a pH gradient across the CM) is due to equilibration of the pH of the cytoplasm with that of the periplasm.

Additional Supporting Figures

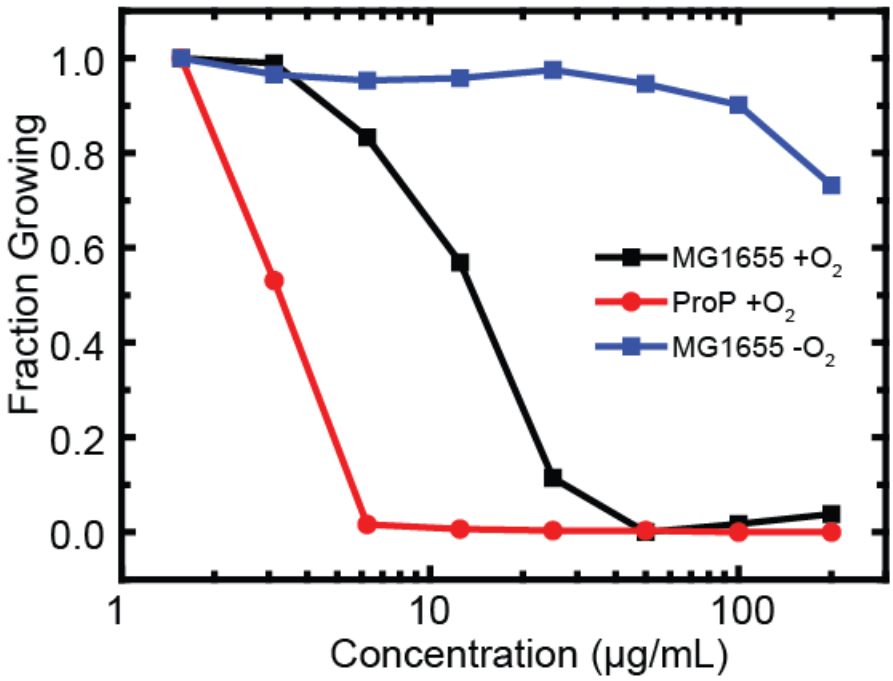

Figure S1. Bulk minimum inhibitory concentration (MIC) assay was performed for **MM$_{63}$:CHx$_{37}$** on "wild type" *E. coli* MG1655 in aerobic (black) and anaerobic (blue) conditions and on the Δ*proP* strain in aerobic condition (red) in EZRDM at 30ºC. Cell growth was measured by optical density (OD) at 595 nm in each well at the 6-hr time point. The data are plotted as *Fraction Growing* = (OD – minOD)/(maxOD – minOD) to enable direct comparison between strains.

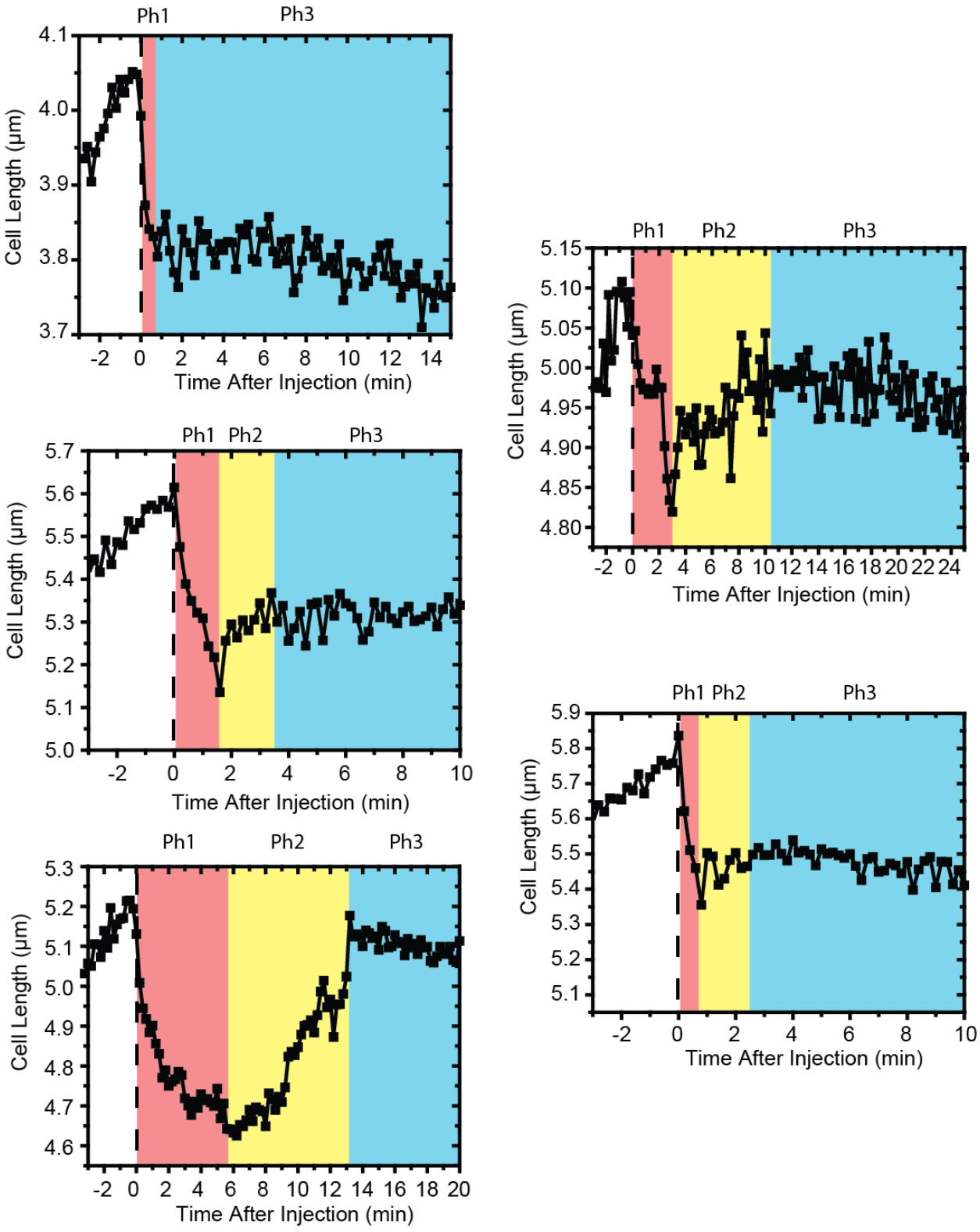

Figure S2. Additional examples of cell length vs time traces for five cells treated with 30 µg/mL of **MM_{63}:CHx_{37}** at *t* = 0. Shrinkage (Phase 1, red), length recovery (Phase 2, yellow), and CM permeabilization (Phase 3, blue) are marked.

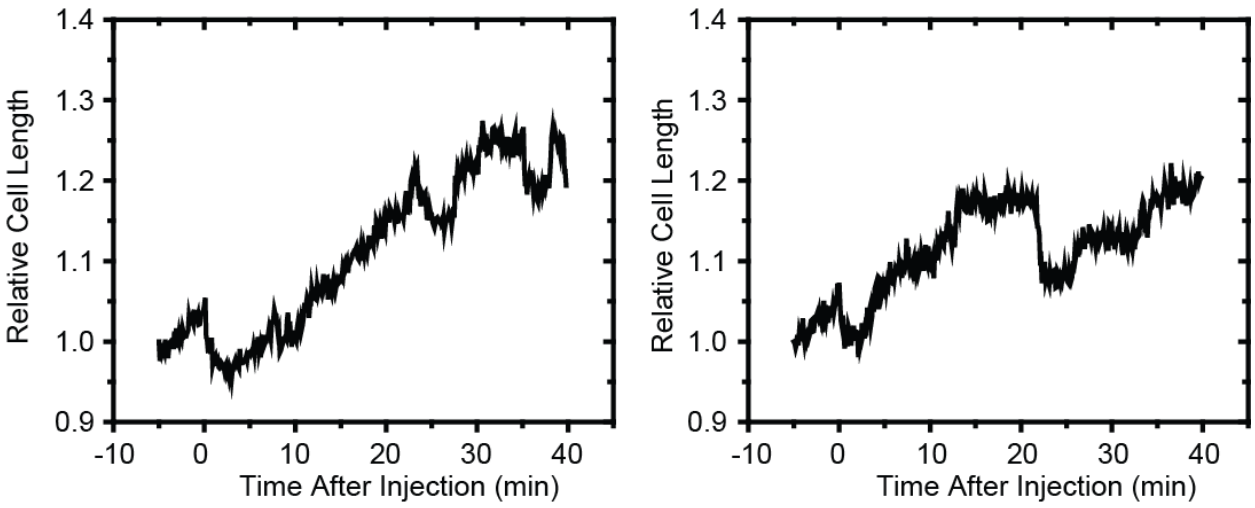

Figure S3. Examples of cells under 30 μg/mL of **MM_{63}:CHx_{37}** that exhibit multiple cycles of shrinkage and periplasmic bubble formation followed by partial recovery. See Movie S2 for an example.

Supporting Movie Details

Movie S1. Phase contrast (left panel) and periplasmic GFP (right panel) movies upon treatment of WT cells with 1.2X MIC (30 μg/mL) **MM_{63}:CHx_{37}** at t = 0. The abrupt cell shrinkage temporally coincides with the formation of periplasmic bubbles at the endcaps immediately after the injection. GFP moves into the cytoplasm after the abrupt cell shrinkage. See Fig. 2 for quantitative details.

Movie S2. Phase contrast (left panel) and periplasmic GFP (right panel) movies upon treatment of WT with 1.2X MIC (30 μg/mL) **MM_{63}:CHx_{37}** at t = 0. The abrupt cell shrinkage temporally coincides with the formation of periplasmic bubbles at the endcaps immediately after the injection. GFP does not move into cytoplasm, but the cell goes through multiple cycles of phase 1 and phase 2. Less than 5% of cells exhibit this behavior.

Movie S3. Phase contrast (left panel) and periplasmic GFP (right panel) movies upon treatment of WT cells with 0.6X MIC (30 μg/mL) **MM_{63}:CHx_{37}** at t = 0. The abrupt cell shrinkage temporally coincides with the formation of periplasmic bubbles at the endcaps immediately after injection. The cell eventually grows, and permeabilization of the CM to GFP does not occur.

Movie S4. Fluorescence images of periplasmic GFP acquired at 10 Hz. WT cells were pre-treated with cephalexin. Injection of **MM_{63}:CHx_{37}** at 1.2X MIC occurred prior to the beginning of the movie. The accumulation of GFP in the endcaps was observed, similar to the effects on cells not treated with cephalexin. Abrupt drainage of GFP from one endcap into the cytoplasm was observed, while GFP at the other endcap persists for ~1 min after drainage of the first endcap. See also Fig. 3.

Movie S5. Phase contrast (left panel) and CellROX* fluorescence (right panel) images of a cell upon treatment with 1.2X MIC (30 μg/mL) **MM_{63}:CHx_{37}**. The injection of **MM_{63}:CHx_{37}** with CellROX at 2.5 μM occurs at t = 0. Fluorescence images were acquired at a rate of 1 frame per 12 s with exposure time of 50 ms for a total of 30 min. Phase contrast images were interleaved at the same rate. The lag between phase contrast and fluorescence images is 6 s. See also Fig. 6.

References for Supporting Information

(1) Sochacki, K. A., Shkel, I. A., Record, M. T., and Weisshaar, J. C. (2011) Protein Diffusion in the Periplasm of E-coli under Osmotic Stress, *Biophys. J. 100*, 22-31.

(2) Baba, T., Ara, T., Hasegawa, M., Takai, Y., Okumura, Y., Baba, M., Datsenko, K. A., Tomita, M., Wanner, B. L., and Mori, H. (2006) Construction of *Escherichia coli* K-12 in-frame, single-gene knockout mutants: the Keio collection, *Molecular Systems Biology 2*, 2006:0008.

(3) Neidhardt, F. C., Bloch, P. L., and Smith, D. F. (1974) Culture medium for enterobacteria, *J Bacteriol 119*, 736-747.

(4) Choi, H., Chakraborty, S., Liu, R., Gellman, S. H., and Weisshaar, J. C. (2014) Medium Effects on Minimum Inhibitory Concentrations of Nylon-3 Polymers against *E. coli*, *PLoS One 9*.

(5) Choi, H., Yang, Z., and Weisshaar, J. C. (2015) Single-cell, real-time detection of oxidative stress induced in *Escherichia coli* by the antimicrobial peptide CM15, *PNAS USA 112*, E303-E310.

(6) Sochacki, K. A., Barns, K. J., Bucki, R., and Weisshaar, J. C. (2011) Real-time attack on single *Escherichia coli* cells by the human antimicrobial peptide LL-37, *PNAS USA108*, E77-E81.

(7) Rangarajan, N., Bakshi, S., and Weisshaar, J. C. (2013) Localized permeabilization of *E. coli* membranes by the antimicrobial peptide Cecropin A, *Biochemistry 52*, 6584-6594.

(8) Trchounian, A., and Kobayashi, H. (1999) Kup is the major K^+ uptake system in *Escherichia coli* upon hyper-osmotic stress at a low pH, *FEBS Lett. 447*, 144-148.

(9) Rhoads, D. B., and Epstein, W. (1977) Energy coupling to net K^+ transport in *Escherichia coli* K-12, *J Biol Chem 252*, 1394-1401.

(10) Siebers, A., and Altendorf, K. (1989) Characterization of the phosphorylated intermediate of the K^+-translocating KDP-ATPase from *Escherichia coli J Biol Chem 264*, 5831-5838.

(11) Buurman, E. T., Kim, K. T., and Epstein, W. (1995) Genetic evidence for two sequentially occupied K^+ binding sites in the KDP transport ATPase, *J Biol Chem 270*, 6678-6685.

(12) Chimerel, C., Field, C. M., Pinero-Fernandez, S., Keyser, U. F., and Summers, D. K. (2012) Indole prevents *Escherichia coli* cell division by modulating membrane potential, *Biochim. Biophys. Acta-Biomembr. 1818*, 1590-1594.

(13) Weber, S. C., Spakowitz, A. J., and Theriot, J. A. (2012) Nonthermal ATP-dependent fluctuations contribute to the *in vivo* motion of chromosomal loci, *PNAS USA 109*, 7338-7343.